Electronic Supplementary Information (ESI)

Controlling the magnitude and polarity of surface charge for PEBA polymer by adding UIO-66 MOFs

Linards Lapčinskis, Andris Šutka, Martynas Kinka, Fa-Kuen Shieh, Līva Ģērmane, Sergejus Balčiūnas, Artis Linarts, and Robertas Grigalaitis

Table S1. Comparison of MOF based TENGs.

Material	Power density
PEBA/UiO-66 this work	47.8 μW cm^{-2}
PEBA/UiO-66-NH_2 this work	13.1 μW cm^{-2}
A-CD-MOF [S1]	8 μW cm^{-2}
Cd-MT [S2]	245.1 μW cm^{-2}
UiO-66–4F@PDMS [S3]	3.87 mW cm^{-2}
ZIF-8 vs Kapton [S4]	39.2 μW cm^{-2}

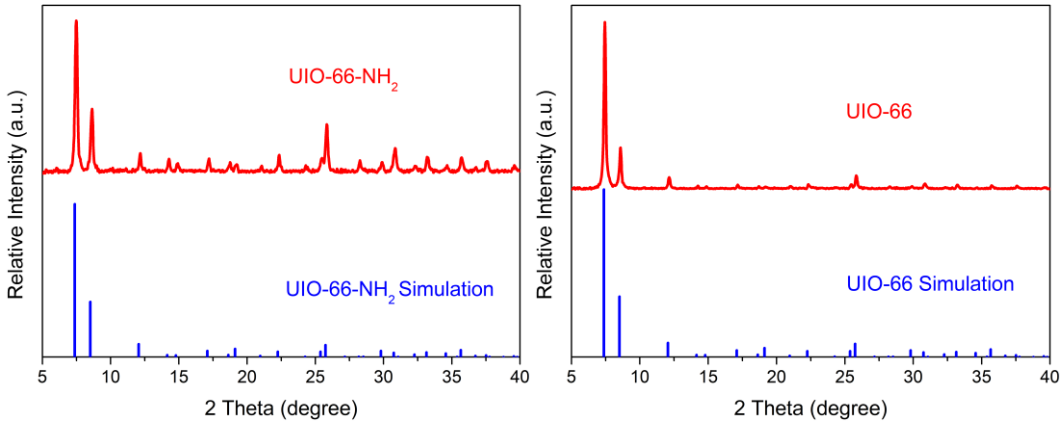

Figure S1. PXRD patterns of the synthesized and simulated UiO-66 and UiO-66-NH_2 MOFs.

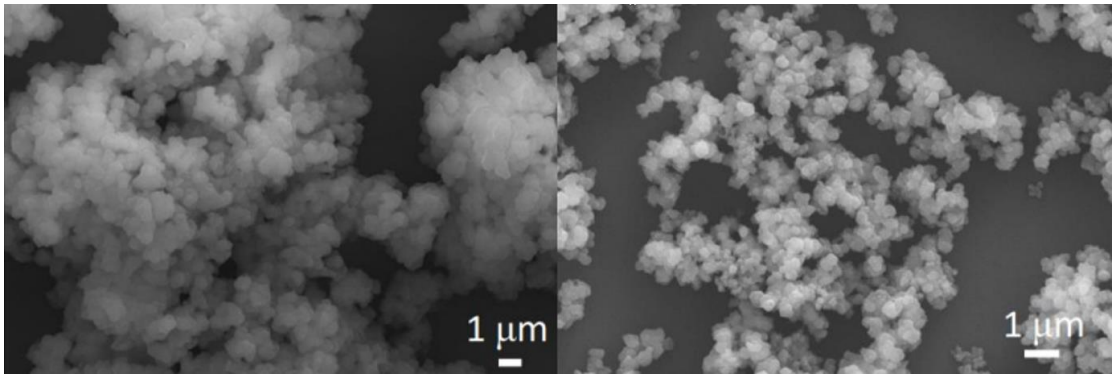

Figure S2. SEM images of UiO-66 (left) and UiO-66-NH_2 (right).

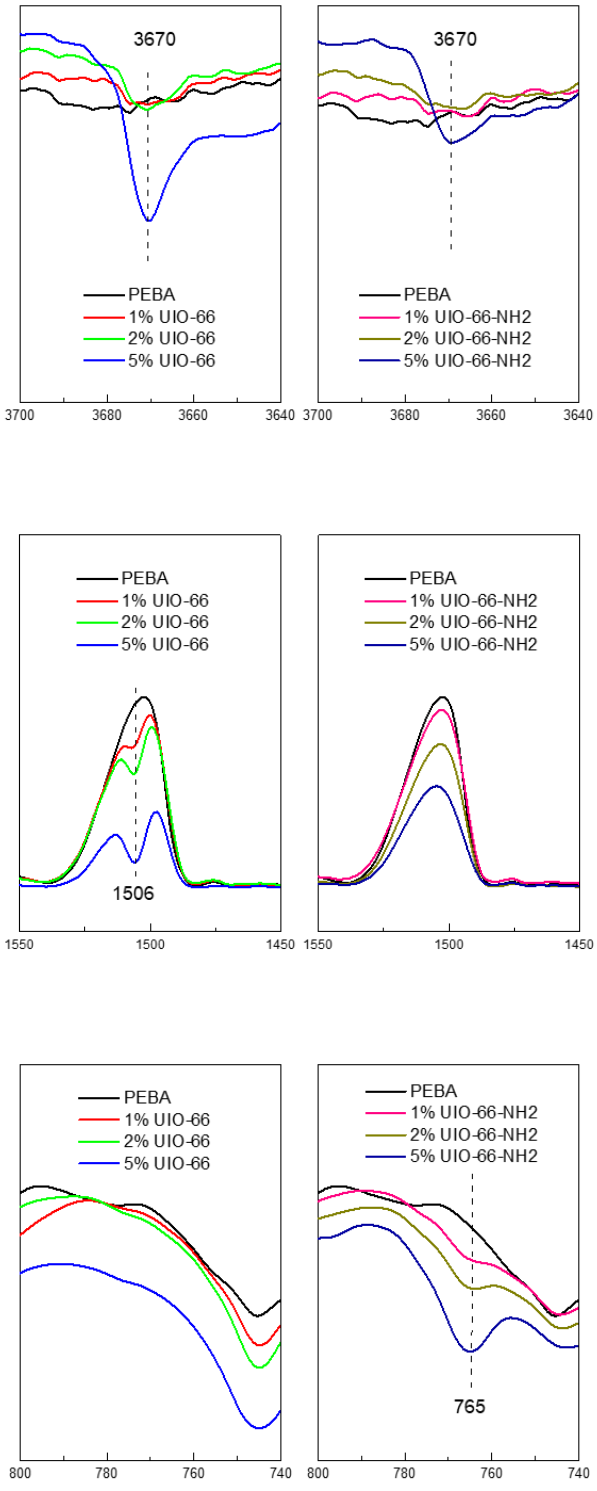

Figure S3. Comparison of infrared transmittance spectra of PEBA/UIO-66 and PEBA/UIO-66-NH2 composites at selected cm^{-1} ranges.

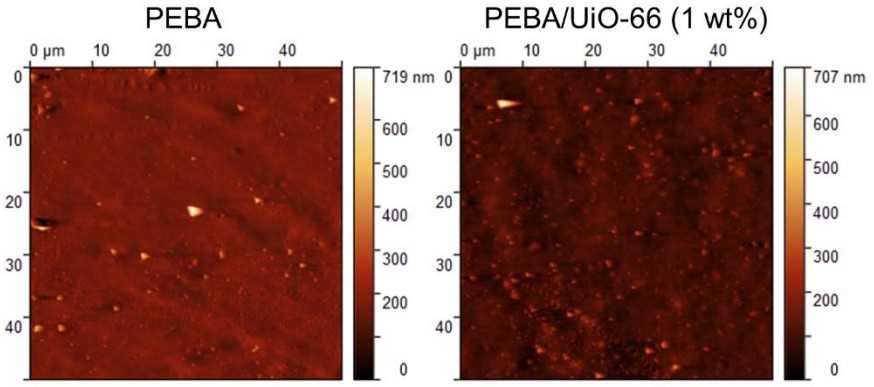

Figure S4. AFM images of pristine PEBA and PEBA/UiO-66 composite layers.

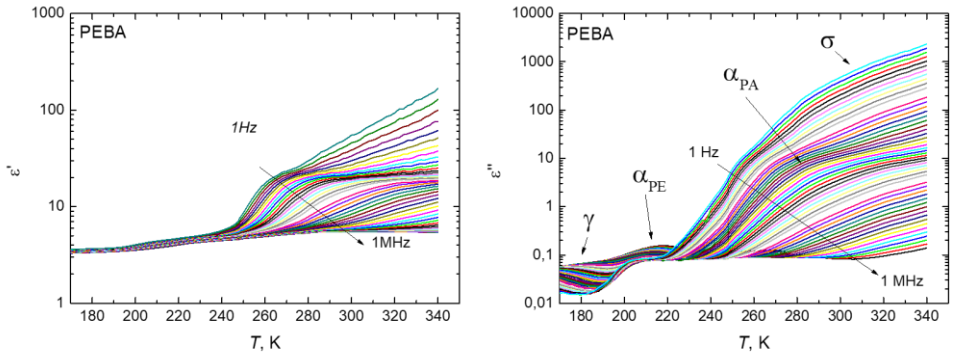

Figure S5. The temperature dependences of the real and imaginary parts of the complex dielectric permittivity of the PEBA polymer during heating at different frequencies.

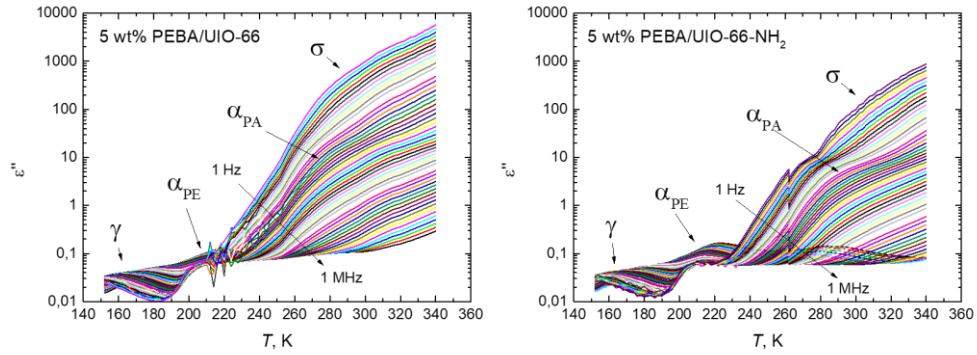

Figure S6. The temperature dependences of the imaginary part of the complex dielectric permittivity of 5 wt.% PEBA/UIO-66 and 5 wt.% PEBA/UIO-66-NH_2 composites during heating at different frequencies. Lower wt.% samples showed similar response.

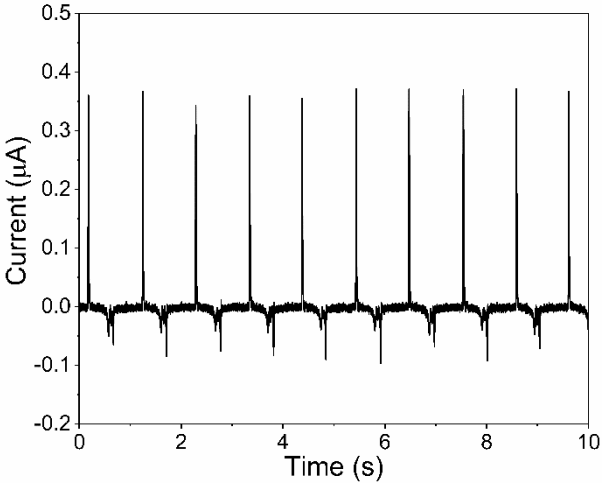

Figure S7. Current peaks measured against ground for PEBA/UiO-66 (0.1 wt.%) composite in contact with ITO.

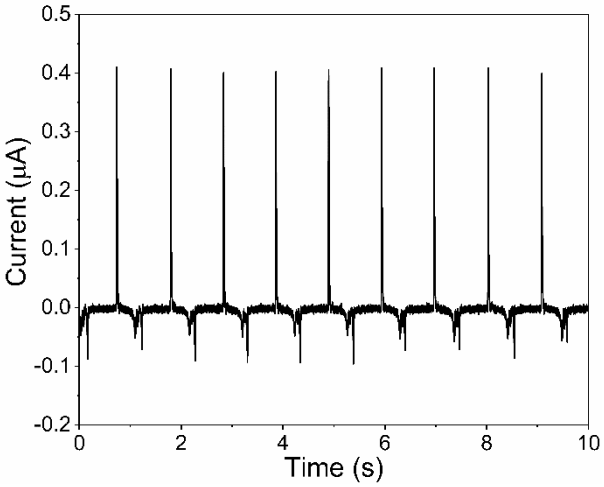

Figure S8. Current peaks measured against ground for PEBA/UiO-66 (0.2 wt.%) composite in contact with ITO.

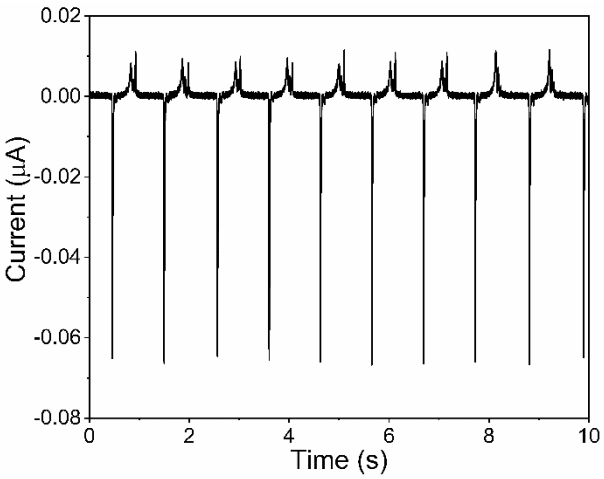

Figure S9. Current peaks measured against ground for PEBA/UiO-66 (0.5 wt.%) composite in contact with ITO.

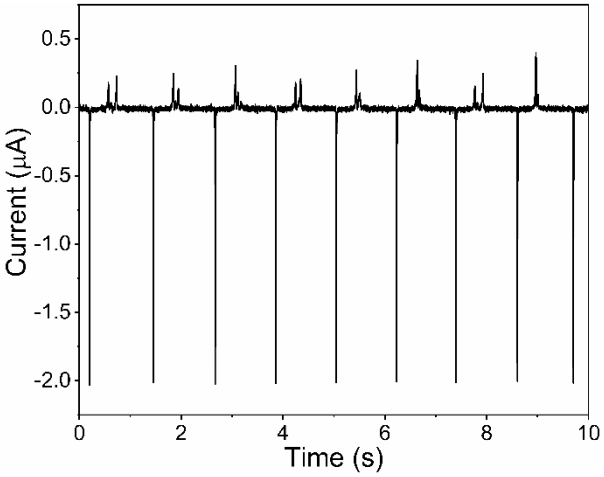

Figure S10. Current peaks measured against ground for PEBA/UiO-66 (1 wt.%) composite in contact with ITO.

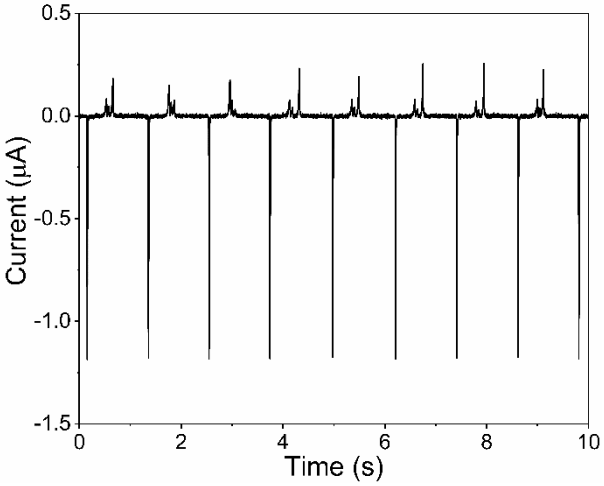

Figure S11. Current peaks measured against ground for PEBA/UiO-66 (2 wt.%) composite in contact with ITO.

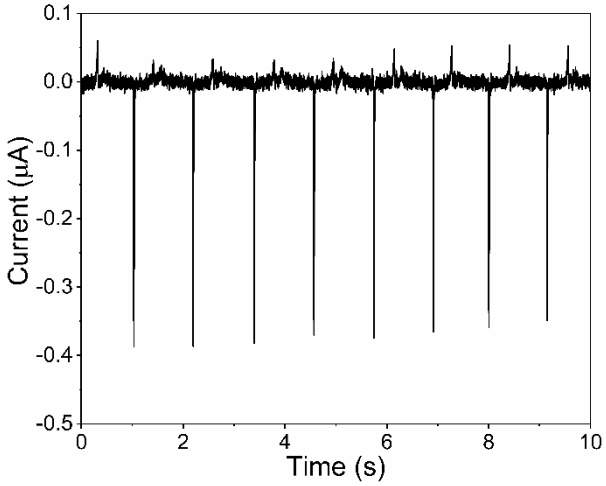

Figure S12. Current peaks measured against ground for PEBA/UiO-66 (5 wt.%) composite in contact with ITO.

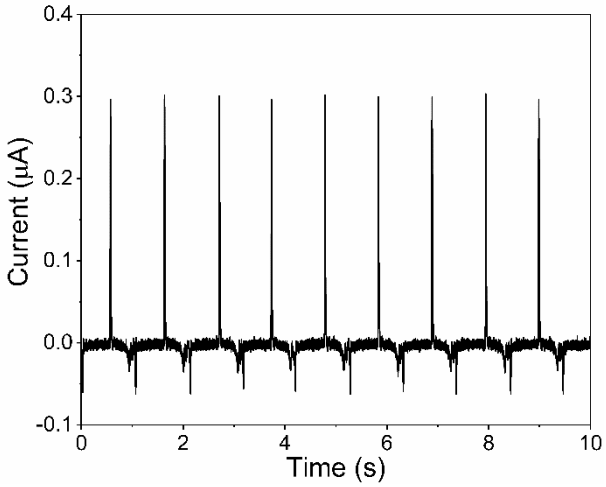

Figure S13. Current peaks measured against ground for PEBA/UiO-66-NH_2 (0.1 wt.%) composite in contact with ITO.

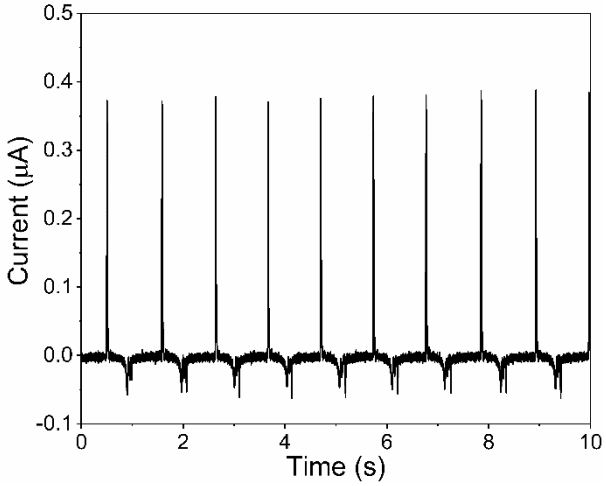

Figure S14. Current peaks measured against ground for PEBA/UiO-66-NH_2 (0.2 wt.%) composite in contact with ITO.

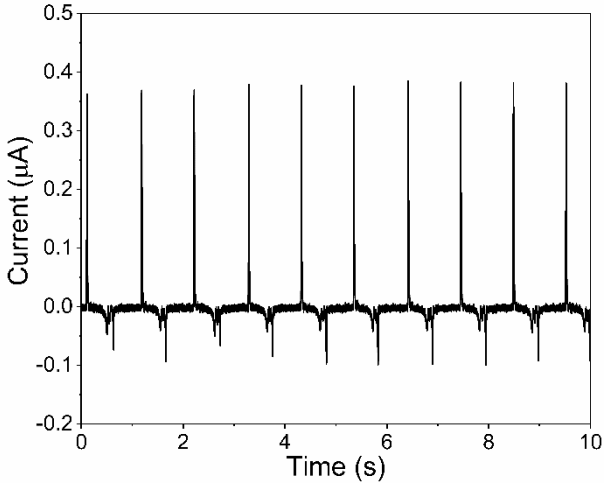

Figure S15. Current peaks measured against ground for PEBA/UiO-66-NH_2 (0.5 wt.%) composite in contact with ITO.

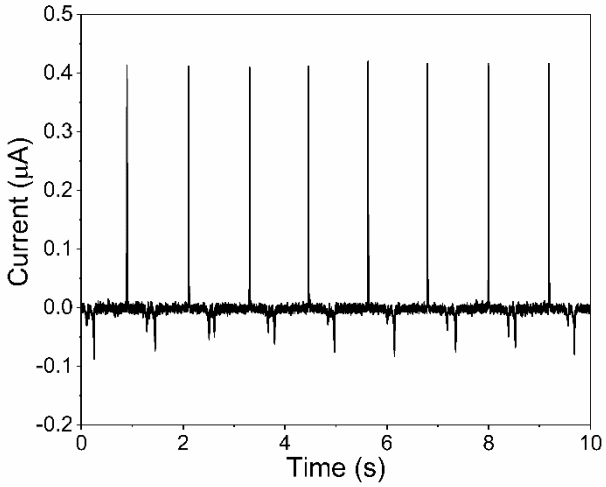

Figure S16. Current peaks measured against ground for PEBA/UiO-66-NH_2 (1 wt.%) composite in contact with ITO.

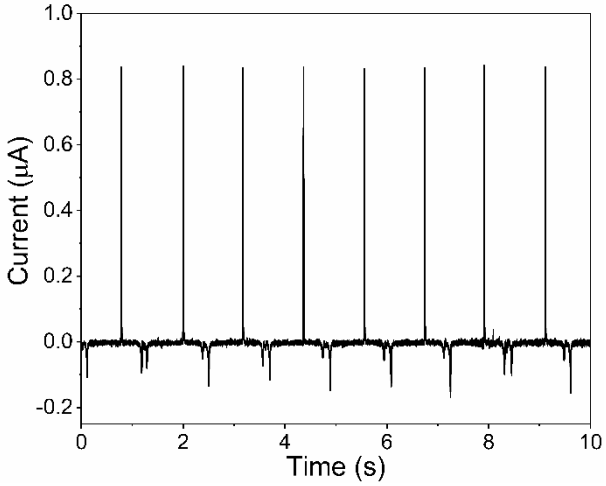

Figure S17. Current peaks measured against ground for PEBA/UiO-66-NH_2 (2 wt.%) composite in contact with ITO.

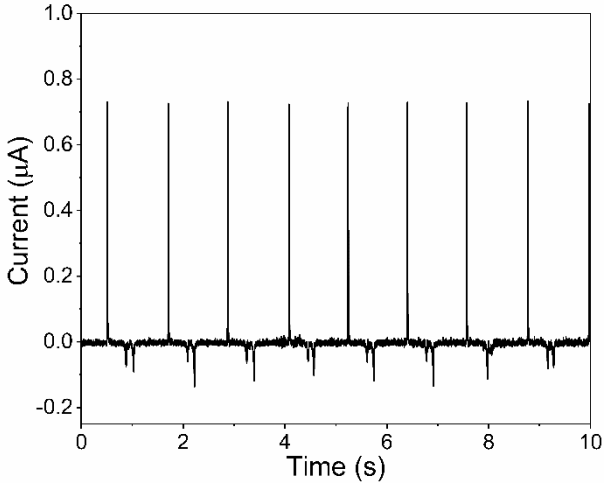

Figure S18. Current peaks measured against ground for PEBA/UiO-66-NH_2 (5 wt.%) composite in contact with ITO.

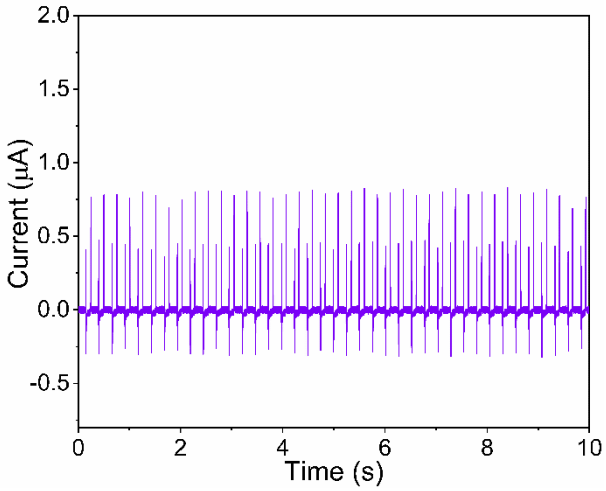

Figure S19. Current peaks measured for TENG constructed using PEBA/UiO-66-NH_2 (2 wt.%) composite and ITO contact layers.

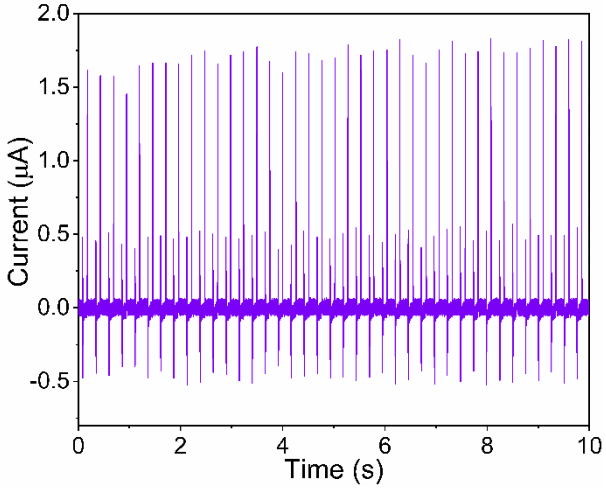

Figure S20. Current peaks measured for TENG constructed using PEBA/UiO-66 (1 wt.%) composite and ITO contact layers.

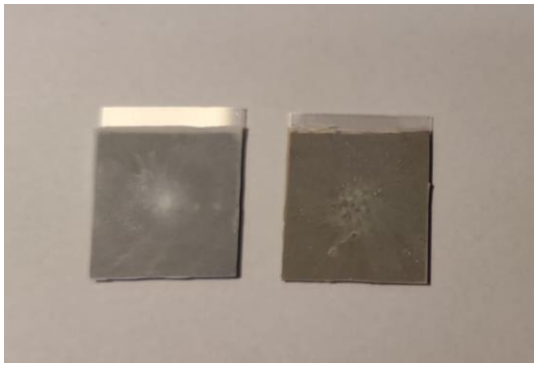

Figure S21. Photos of PEBA films covered by UiO-66 (left) and UiO-66-NH_2 (right) MOF particles.

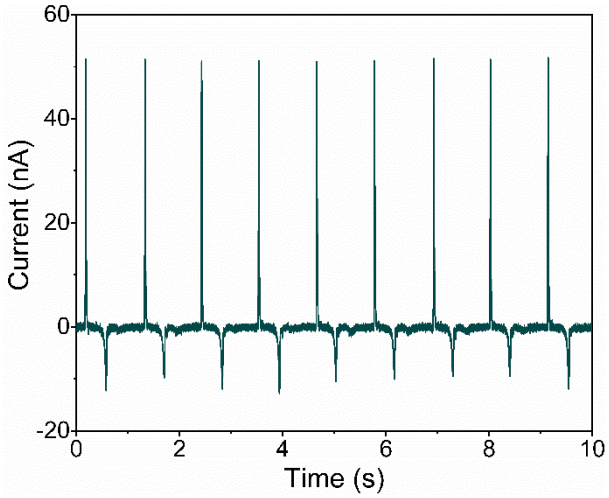

Figure S22. Current peaks measured for PEBA film covered by UiO-66-NH_2 in contact with ITO.

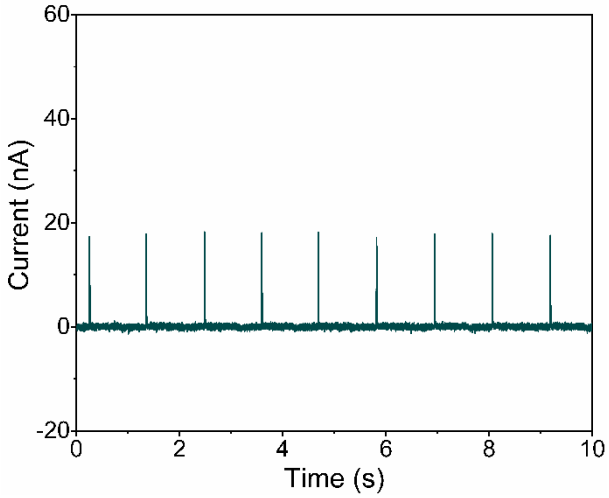

Figure S23. Current peaks measured for PEBA film covered by UiO-66 in contact with ITO.

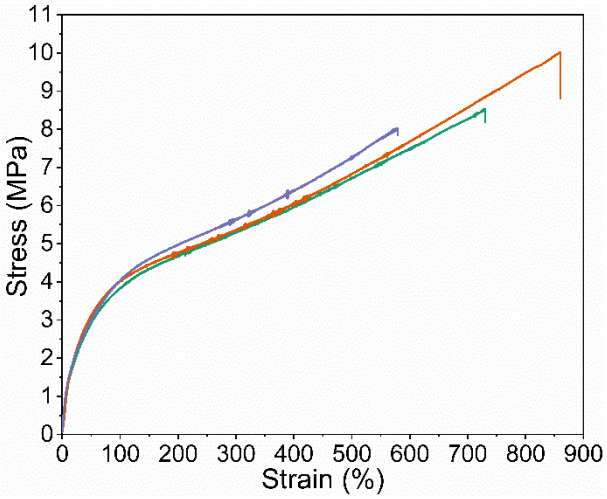

Figure S24. Stress-strain curves obtained from tensile tests of three PEBA/UiO-66 (1 wt%) composite samples.

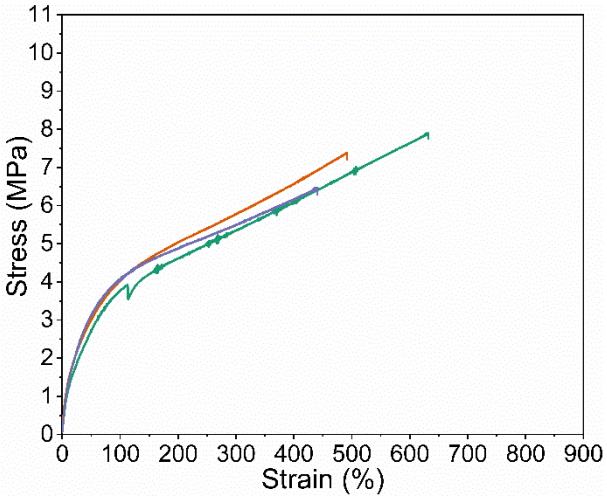

Figure S25. Stress-strain curves obtained from tensile tests of three PEBA/UiO-66-NH_2 (2 wt%) composite samples.

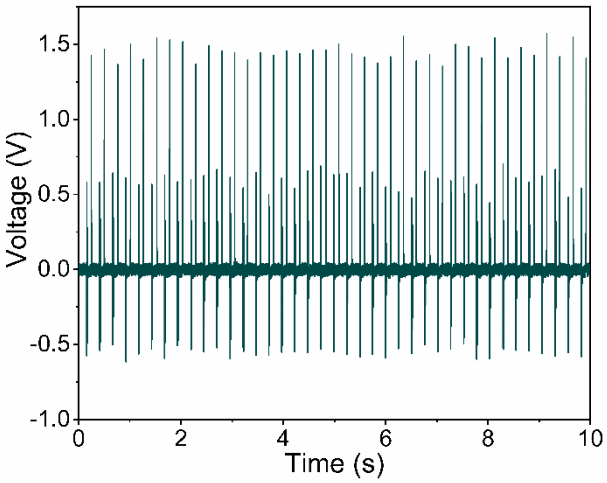

Figure S26. Voltage peaks measured at 500 kΩ load resistance for TENG based on PEBA/UiO-66-NH_2 (2 wt.%) composite and ITO contact layers.

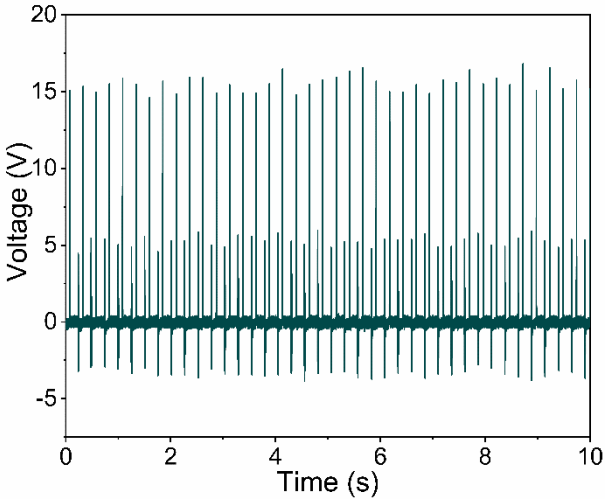

Figure S27. Voltage peaks measured at 4.7 MΩ load resistance for TENG based on PEBA/UiO-66-NH_2 (2 wt.%) composite and ITO contact layers.

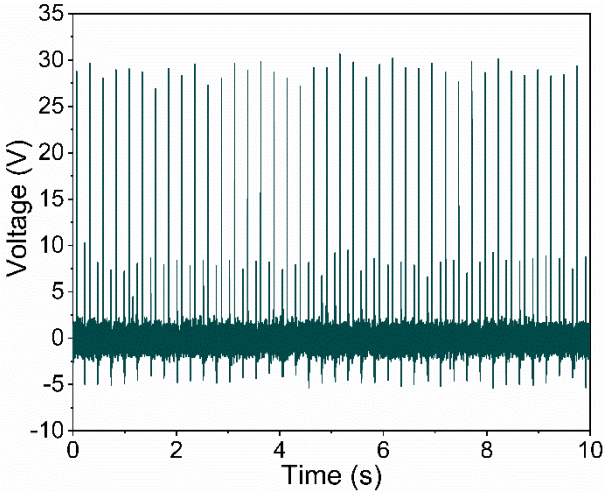

Figure S28. Voltage peaks measured at 10 MΩ load resistance for TENG based on PEBA/UiO-66-NH_2 (2 wt.%) composite and ITO contact layers.

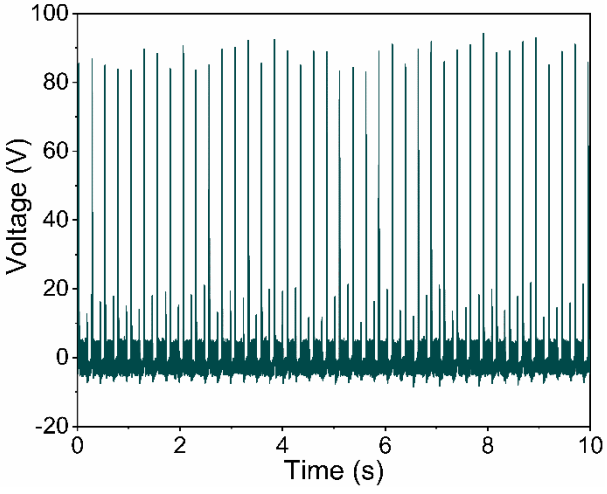

Figure S29. Voltage peaks measured at 100 MΩ load resistance for TENG based on PEBA/UiO-66-NH_2 (2 wt.%) composite and ITO contact layers.

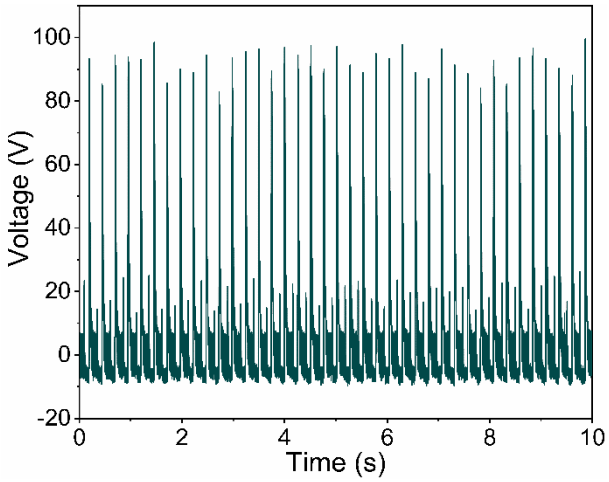

Figure S30. Voltage peaks measured at 550 MΩ load resistance for TENG based on PEBA/UiO-66-NH_2 (2 wt.%) composite and ITO contact layers.

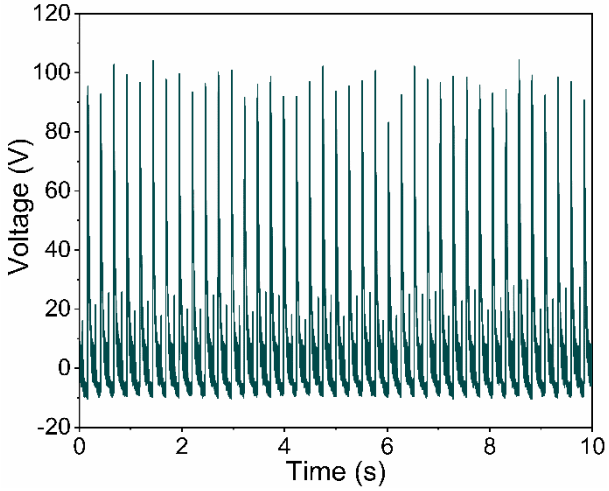

Figure S31. Voltage peaks measured at 1 GΩ load resistance for TENG based on PEBA/UiO-66-NH_2 (2 wt.%) composite and ITO contact layers.

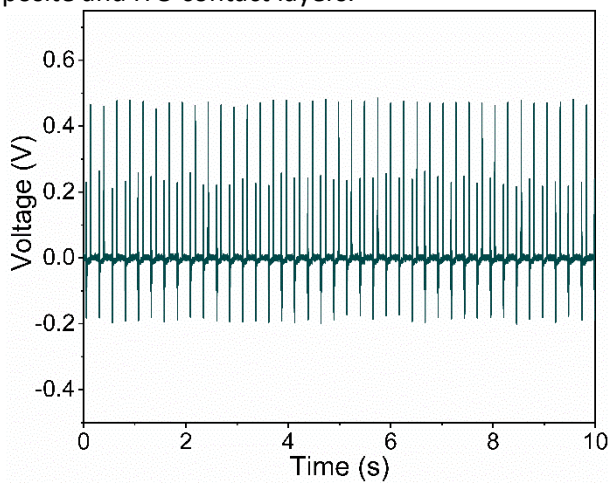

Figure S32. Voltage peaks measured at 500 kΩ load resistance for TENG based on PEBA/UiO-66 (1 wt.%) composite and ITO contact layers.

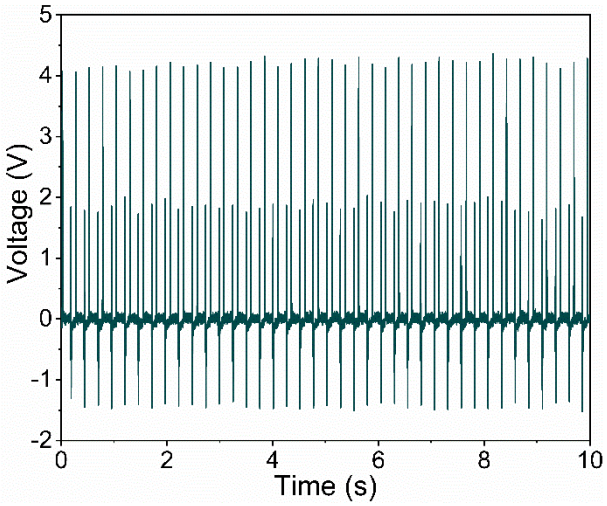

Figure S33. Voltage peaks measured at 4.7 MΩ load resistance for TENG based on PEBA/UiO-66 (1 wt.%) composite and ITO contact layers.

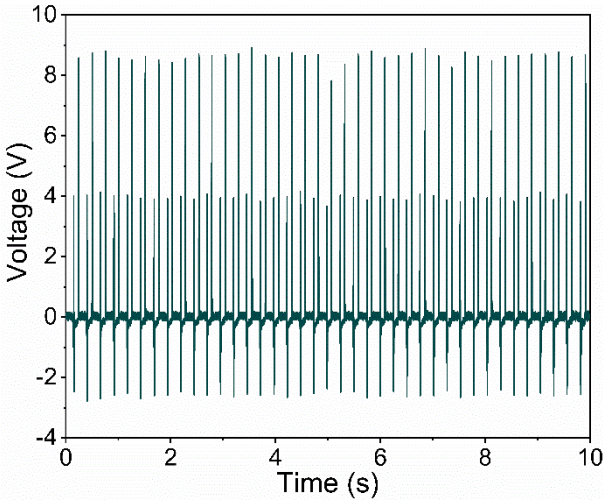

Figure S34. Voltage peaks measured at 10 MΩ load resistance for TENG based on PEBA/UiO-66 (1 wt.%) composite and ITO contact layers.

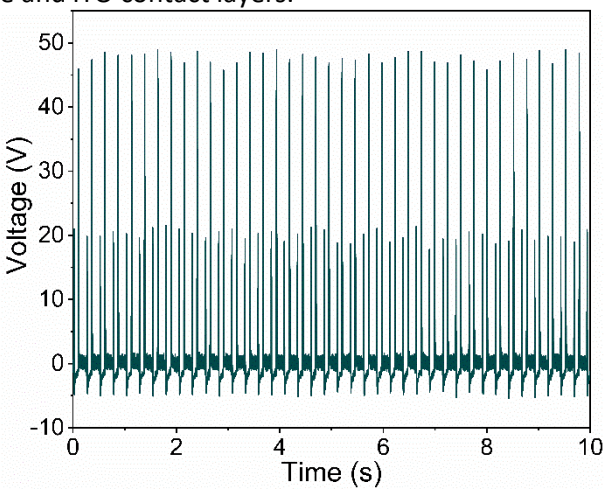

Figure S35. Voltage peaks measured at 100 MΩ load resistance for TENG based on PEBA/UiO-66 (1 wt.%) composite and ITO contact layers.

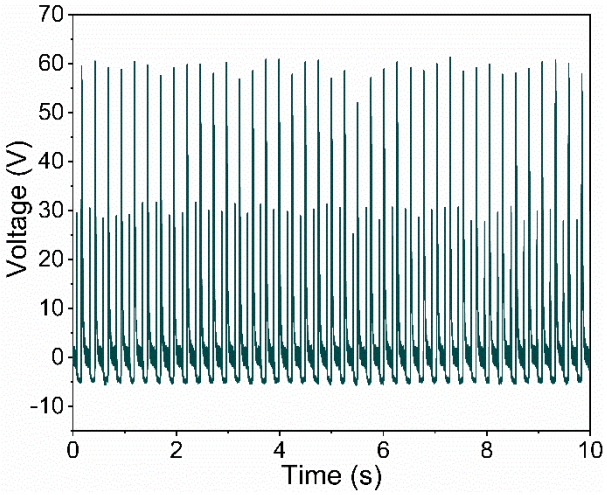

Figure S36. Voltage peaks measured at 550 MΩ load resistance for TENG based on PEBA/UiO-66 (1 wt.%) composite and ITO contact layers.

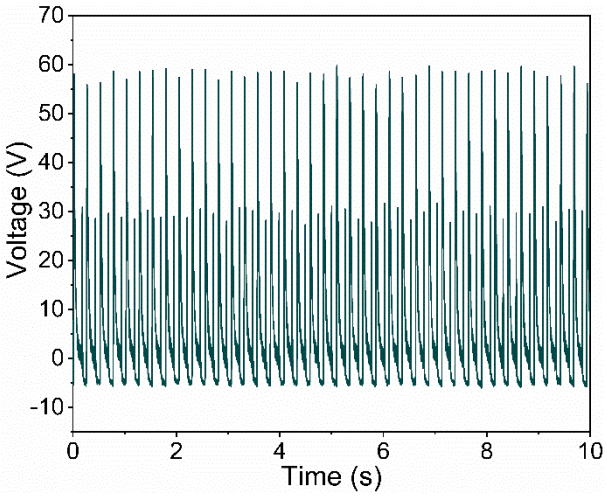

Figure S38. Voltage peaks measured at 1 GΩ load resistance for TENG based on PEBA/UiO-66 (1 wt.%) composite and ITO contact layers.

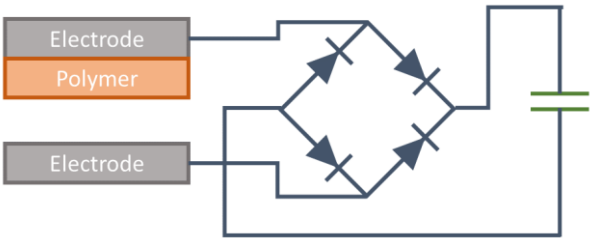

Figure S39. Schematic of TENG connected to capacitor via full bridge rectifier.

Supplementary references

[S1] K. Gao, J. Chen, M. Zhao, R. Hu, S. Chen, X. Xue, Z. Shao and H. Hou, *Dalton Trans.*, 2023, **52**, 444-451

[S2] S. Hajra, M. Sahu, A.M. Padhan, I.S. Lee, D.K. Yi, P. Alagarsamy, S.S.Nanda, and H.J. Kim, *Adv. Funct. Mater.* 2021, **31**, 2101829

[S3] Y.-M. Wang, X. Zhang, C. Liu, L. Wu, J. Zhang, T. Lei, Y. Wang, X.-B. Yin, R. Yang, *Nano Energy*, 2023, **107**, 108149

[S4] G. Khandelwal, A. Chandrasekhar, N. P. Maria Joseph Raj, S.-J. Kim, *Adv. Energy Mater.* 2019, **9**, 1803581.